© 2021. Published by The Company of Biologists Ltd | Development (2021) 148, dev200029. doi:10.1242/dev.200029

TECHNIQUES AND RESOURCES

RESEARCH REPORT

# High-resolution dynamic mapping of the *C. elegans* intestinal brush border

**Aurélien Bidaud-Meynard[1], Flora Demouchy[1,*], Ophélie Nicolle[1,*], Anne Pacquelet[1,*], Shashi Kumar Suman[2], Camille N. Plancke[2], François B. Robin[2] and Grégoire Michaux[1,‡]**

## ABSTRACT

The intestinal brush border is made of an array of microvilli that increases the membrane surface area for nutrient processing, absorption and host defense. Studies on mammalian cultured epithelial cells have uncovered some of the molecular players and physical constraints required to establish this apical specialized membrane. However, the building and maintenance of a brush border *in vivo* has not yet been investigated in detail. Here, we combined super-resolution imaging, transmission electron microscopy and genome editing in the developing nematode *Caenorhabditis elegans* to build a high-resolution and dynamic localization map of known and new brush border markers. Notably, we show that microvilli components are dynamically enriched at the apical membrane during microvilli outgrowth and maturation, but become highly stable once microvilli are built. This new toolbox will be instrumental for understanding the molecular processes of microvilli growth and maintenance *in vivo*, as well as the effect of genetic perturbations, notably in the context of disorders affecting brush border integrity.

**KEY WORDS: Brush border, Intestine, Microvilli, Polarity**

## INTRODUCTION

Intestinal microvilli are essential for nutrient absorption. They are organized into a well-ordered and tightly packed array by F-actin crosslinking and bundling factors, such as villin, espin and plastin 1 (also known as fimbrin) (Sauvanet et al., 2015). Recent studies in epithelial cell lines have identified new functional players, such as IRTKS (also known as Baiap2l1) and myosin 1a/6/7b (Crawley et al., 2014a; Postema et al., 2018), and new mechanisms of brush border assembly and maintenance by vesicular trafficking (Vogel et al., 2015), microvilli motility, contraction and clustering (Meenderink et al., 2019; Chinowsky et al., 2020) or intermicrovillar protocadherin bridges (Crawley et al., 2014b). Additionally, live imaging has revealed some of the key initiation and maturation steps of microvilli biogenesis in cell lines (Gaeta et al., 2021). However, a description of brush border formation and maintenance *in vivo* is lacking.

[1]Université de Rennes, CNRS, IGDR (Institut de Génétique et Développement de Rennes) - UMR 6290, F-35000 Rennes, France. [2]Sorbonne Université, Institut Biologie Paris Seine, CNRS UMR7622, Developmental Biology Laboratory, Inserm U1156, F-75005 Paris, France.
*These authors contributed equally to this work

‡Author for correspondence (gmichaux@univ-rennes1.fr)

A.B., 0000-0003-0103-3827; F.D., 0000-0001-5162-9974; A.P., 0000-0001-5923-4619; F.B.R., 0000-0002-2420-2593; G.M., 0000-0003-1222-5461

**Handling Editor: Swathi Arur**
**Received 26 July 2021; Accepted 4 October 2021**

*Caenorhabditis elegans* has been widely used as an *in vivo* model of intestinal luminogenesis, polarity and host defense (Zhang et al., 2013; Zhang and Hou, 2013; Sato et al., 2014). Intestinal organogenesis encompasses cell division and intercalation steps from the E blastomere to generate 20 perennial cells arranged into nine rings forming an ellipse-shaped tube that runs along the body of the worm (Leung et al., 1999; Asan et al., 2016). Cell polarization begins at the E16 stage with cellular component relocalization and cell shape changes (Leung et al., 1999), as well as apical accumulation of the polarity determinant PAR-3, which recruits the other members of the PAR module (Feldman and Priess, 2012; Achilleos et al., 2010). Luminogenesis occurs concomitantly with the formation of apical cavities at the midline that ultimately form a lumen (Leung et al., 1999). *C. elegans* enterocytes display a brush border that is structurally similar to that of mammals (Leung et al., 1999; Geisler et al., 2019; Bidaud-Meynard et al., 2019): microvilli are made of F-actin core bundles, notably the intestinal-specific actin isoform *act-5*, depletion of which results in a circular lumen with sparse and defective microvilli (MacQueen et al., 2005). Several F-actin regulators are essential for *C. elegans* brush border integrity, including ERM-1, the Ezrin/Radixin/Moesin only ortholog (Gobel et al., 2004; Van Furden et al., 2004), and the actin-capping factor EPS-8 (Croce et al., 2004). As in mammals, microvilli are anchored on a terminal web composed of a network of F-actin and an endotube made of intermediate filaments, in which IFB-2 plays a major role (Geisler et al., 2020; Bossinger et al., 2004). Here, we combined super-resolution and quantitative live microscopy, transmission electron microscopy (TEM) and fluorescence recovery after photobleaching (FRAP) data to characterize the recruitment and dynamics of endogenously tagged markers during the establishment of the *C. elegans* brush border. In particular, we show that intestinal microvilli form and grow throughout embryonic and larval development but are highly stable once formed.

## RESULTS AND DISCUSSION

### TEM analysis of brush border establishment in the *C. elegans* developing embryo

We first characterized the assembly of the brush border during *C. elegans* development by TEM (Nicolle et al., 2015). *C. elegans* embryonic morphogenesis is staged according to the shape and elongation of the embryo, passing through ‘lima bean’ [360 min post-fertilization (mpf)] and ‘comma’ (430 mpf) stages, after which embryos elongate and fold one and a half (460 mpf), two (490 mpf), three (550 mpf) and four times before hatching (L1 stage, 840 mpf). Adulthood is then reached after three consecutive molts, defining the L2 [~21 h post-fertilization (hpf)], L3 (~29 hpf) and L4 (~39 hpf) larval stages (Altun and Hall, 2009). We observed that the intestinal lumen starts to open at the comma stage and progressively expands to reach an elliptical shape in larvae

Development (2021) 148, dev200029. doi:10.1242/dev.200029

(Fig. 1A,B). The first microvilli-like membrane extensions were observed at the 1.5-fold stage and started to cover the apex with a disorganized pattern at the 2.5-fold stage, to finally form a regular brush border from the 3-fold stage (Fig. 1A). Measurements suggested a relatively continuous increase in microvilli density, length and width (Fig. 1A-E, Fig. S1A-C), implying a gradual maturation of the brush border and *de novo* growth of microvilli throughout development to fill in the membrane added during intestinal surface expansion (Fig. 1A, arrows). Finally, transversal imaging of the brush border allowed measurement of the distance between microvilli edges and centers (76.0±1.1 nm and 203.2 ±2.0 nm, respectively) (Fig. 1F,G).

### Dynamic recruitment of brush border components during *C. elegans* development

Expression profiling in mammalian enterocytes between the proliferative crypt and the terminally differentiated villus demonstrated a marked upregulation of actin cytoskeleton-related genes, including actin, ezrin, villin and espin (Chang et al., 2008; Mariadason et al., 2005). Notably, recent data in LLC-PK1 cells showed a stepwise recruitment of EPS8 and IRTKS first, and then ezrin, during microvilli outgrowth (Gaeta et al., 2021). To perform a similar analysis, we systematically investigated the expression and apical localization of endogenously tagged new and known brush border markers.

Although the ortholog of villin is not localized at the brush border (Hunt-Newbury et al., 2007) and espin does not have a *C. elegans* ortholog, we found that PLST-1, the ortholog of plastin 1/fimbrin (Fig. 2A, Fig. S2), one of the major F-actin organizing factors in mammalian brush borders (Crawley et al., 2014a), was apically localized. Second, the F-actin cross-linker FLN-2 (the ortholog of filamin A), which has been proposed to control brush border maintenance in mammalian models (Zhou et al., 2014), was also observed at the enterocyte apical membrane (Fig. 2B, Fig. S2).

In addition, many members of the myosin superfamily of actin motors have been localized to the brush border in mammalian cells (McConnell et al., 2011; Sauvanet et al., 2015). This superfamily comprises 12 classes of conventional and unconventional myosins, which function as multimers of heavy and light chains (Fili and Toseland, 2019). In the brush border, they have been shown to fulfil structural (e.g. MYO7b, MYH14), trafficking (e.g. MYO-1a, -6) or contractile (non-muscle myosin NM2C) functions (Houdusse and Titus, 2021; Chinowsky et al., 2020). We found that a specific set of myosins accumulates at the enterocyte apex throughout *C. elegans* development: (1) the unconventional heavy chain HUM-5 (the ortholog of human MYO1d/g), which is also localized at the lateral membrane (Fig. 2C, Fig. S2), but not the other members of this class, HUM-1 and HUM-2 (Fig. S3A,B); (2) the essential myosin light chain MLC-5 (Gally et al., 2009) (the ortholog of human MYL1/6) accumulated at the apical membrane in both embryos and larvae (Fig. 2D, Fig. S2), whereas MLC-4 was only weakly expressed in embryos (Fig. S3C). Interestingly, we found that NMY-1 and NMY-2 (the orthologs of the non-muscle myosins NM2A/B and NM2B/C, respectively) (Fig. S3D,E), did not accumulate apically, or accumulated only very weakly, which indicates that myosin-dependent contractility may be less crucial for microvilli assembly in *C. elegans* than in mammals (Chinowsky et al., 2020). These results suggest species-specific mechanisms or compensation between myosins, as shown before (Houdusse and Titus, 2021), and the need for systematic approaches to characterize better the components of brush borders, for instance to identify putative protocadherin-based intermicrovillar bridges molecules (Crawley et al., 2014b) among the various cadherin-like proteins in the *C. elegans* genome (Loveless and Hardin, 2012).

To assess quantitatively the expression of these apically enriched factors during brush border establishment, we used photon counting detectors and quantified the absolute apical signal of endogenously tagged proteins throughout *C. elegans* development (Fig. 2S, Figs S2, S3F). We observed that a set of markers was already localized at the apical membrane at the lima bean stage, before microvilli onset: PLST-1, FLN-2, ERM-1 and ACT-5 (note that ACT-5 was exogenously expressed under its own promoter, because of the embryonic lethality of endogenously tagged strains), as well as the intermediate filament IFB-2, which appears slightly later (Fig. 2E-J, Fig. S2). Then, we observed that the apical localization of these markers, as well as that of EPS-8, HUM-5 and MLC-5, dramatically increased concomitantly with microvilli assembly (from the 1.5-fold stage), and that most of them peaked between the 4-fold and L1 stages to then decrease until adulthood (Fig. 2K-S, Fig. S2). The early apical accumulation of some of these factors might reflect their importance for microvilli assembly, which is consistent with the requirement of ERM-1 and ACT-5 (Gobel et al., 2004; MacQueen et al., 2005) and the direct relationship between G-actin apical availability and microvilli growth (Faust et al., 2019). As PLST-1 accumulated before microvilli onset, it could also play a role in microvilli initial assembly *in vivo*, which is coherent with the disorganized terminal web and microvilli rootlets described in *Pls1* knockout mice (Grimm-Gunter et al., 2009), despite no obvious defect in *plst-1 C. elegans* mutants at larval stages (Fig. S3G). Interestingly, we observed that FLN-2 displayed a shifted pattern, with an early peak that may suggest a specific role in microvilli establishment. Thus, an evolving set of factors might control microvilli building in *C. elegans*: a 'pre-assembly module', composed, at least, of ERM-1, ACT-5, PLST-1, FLN-2 and IFB-2; an 'assembly module', composed additionally of EPS-8, HUM-5 and MLC-5, and, finally, a 'mature module' that does not require FLN-2 (Fig. S5B).

### Super-resolution imaging of the brush border *in vivo*

According to the Rayleigh criterion $\left(\text{Rfluo} = \frac{1.22}{2 \times \text{NA}}\right)$, the optical axial resolution of the 405, 488 and 561 nm lasers is 176.5, 212.6 and 244.4 nm, respectively, using an NA1.4 objective, which is above the limit to resolve individual microvilli (~100 nm between edges, Fig. 1E,G). To test this, we endogenously tagged ERM-1 with three different fluorophores: Blue Fluorescent Protein (mTagBFP2/BFP, $\lambda_{Ex}$381 nm/$\lambda_{Em}$445 nm) (Subach et al., 2011), mNeongreen (mNG, $\lambda_{Ex}$506 nm/$\lambda_{Em}$517 nm) (Shaner et al., 2013) and wrmScarlet (wSc, $\lambda_{Ex}$569 nm/$\lambda_{Em}$593 nm) (El Mouridi et al., 2017) and imaged them with a multi-detector and deconvolution-based super-resolution imaging system (see Materials and Methods). We could visualize the regular alignment of microvilli with BFP and mNG tags, but it was less visible with the wSc fluorophore (Fig. 3A,B). In addition to individual microvilli, we could also precisely localize brush border markers along the microvilli long axis. Indeed, whereas ERM-1 covered the whole microvilli length, the chloride intracellular channel 2 (CLIC-2) ortholog EXL-1 (Liang et al., 2017) accumulated at the tip of microvilli (Fig. 3C) and the P-GlycoProtein related transporter PGP-1 at their base (Bidaud-Meynard et al., 2019). Of note, this method allowed us to uncover localization differences between in-locus mNG-tagged and overexpressed GFP-tagged proteins (compare Fig. 3C with Fig. S4A), as already reported for E-cadherin in the same tissue (Cordova-Burgos et al., 2021).

Development (2021) 148, dev200029. doi:10.1242/dev.200029

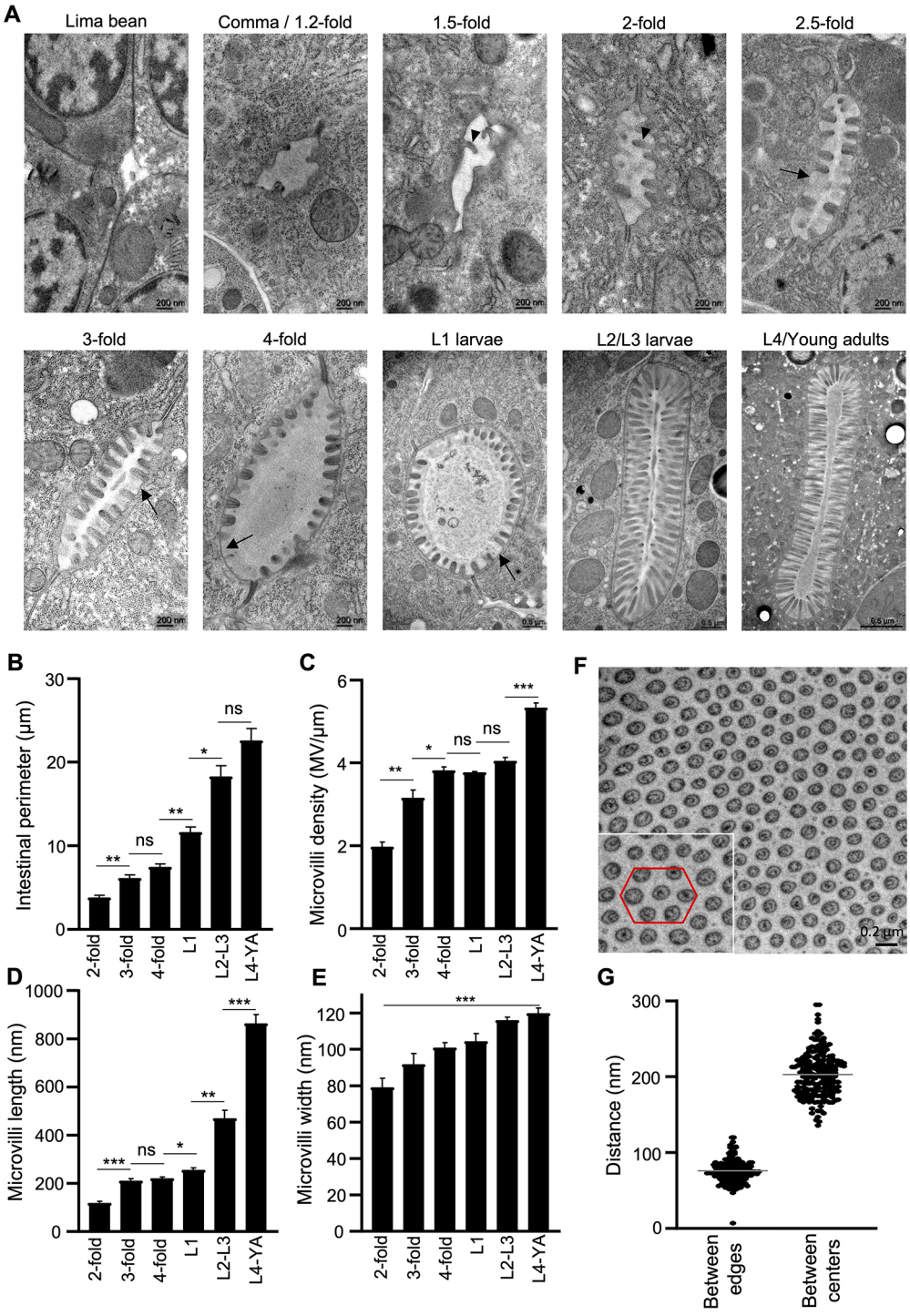


**Fig. 1. TEM analysis of the brush border.** (A) Representative TEM images of *C. elegans* intestinal lumen at the developmental stages indicated. Arrowheads indicate nascent microvilli; arrows indicate empty spaces between microvilli. (B-E) Quantification of the lumen perimeter (B) and microvilli density (C), length (D) and width (E) from TEM images. Histograms show the mean±s.e.m. of an average of 3-13 slices (B), 3-13 lumen (C) and 6-29 microvilli (D-E) per sample from three to five worms at each developmental stage. YA, young adults. ns, non-significant. **P*<0.05, ***P*<0.01, ****P*<0.001. Statistical significance was calculated using unpaired Student's *t*-test except in C (4-fold versus L1 and L1 versus L2-L3), where a Mann–Whitney test was used due to a non-normal data distribution. (F) Transversal view of the brush border in an L4 worm illustrating microvilli hexagonal packing. Inset shows magnification of the boxed area with the putative hexagonal organization of microvilli highlighted by the red line. (G) The distance between microvilli edges and centers was calculated on 200 microvilli from two L4 larvae.

Individual microvilli were similarly visualized using random illumination microscopy (Mangeat et al., 2021), but not using conventional confocal or stimulated-emission-depletion microscopes (Fig. S4B). The brush border could also be imaged transversally (compare Figs 3D and 1F). Hence, the combination of a super-resolution imaging system, appropriate fluorophores and endogenous expression allows the visualization of individual microvilli in *C. elegans* intestine.

We then used these tools to characterize the (co)localization of known and newly identified apical markers in adult worms. Using a strain co-expressing endogenously tagged versions of two classical brush border markers, ERM-1 and EPS-8, and the endotube's intermediate filament IFB-2, we observed that ERM-1 localized along the whole microvilli but not in the terminal web (Fig. 3E). EPS-8 accumulated at the tip of the microvilli, where it partially colocalized with ERM-1, and was also found marginally at the terminal web vicinity, as observed previously by immuno-electron microscopy (Croce et al., 2004) (Fig. 3E). Finally, we were able to resolve in some worms the difference between exogenously expressed ACT-5, which localized along and at the base of the microvilli, and the endotube marker IFB-2 (Geisler et al., 2019; Bossinger et al., 2004) (Fig. S4C).

Development (2021) 148, dev200029. doi:10.1242/dev.200029

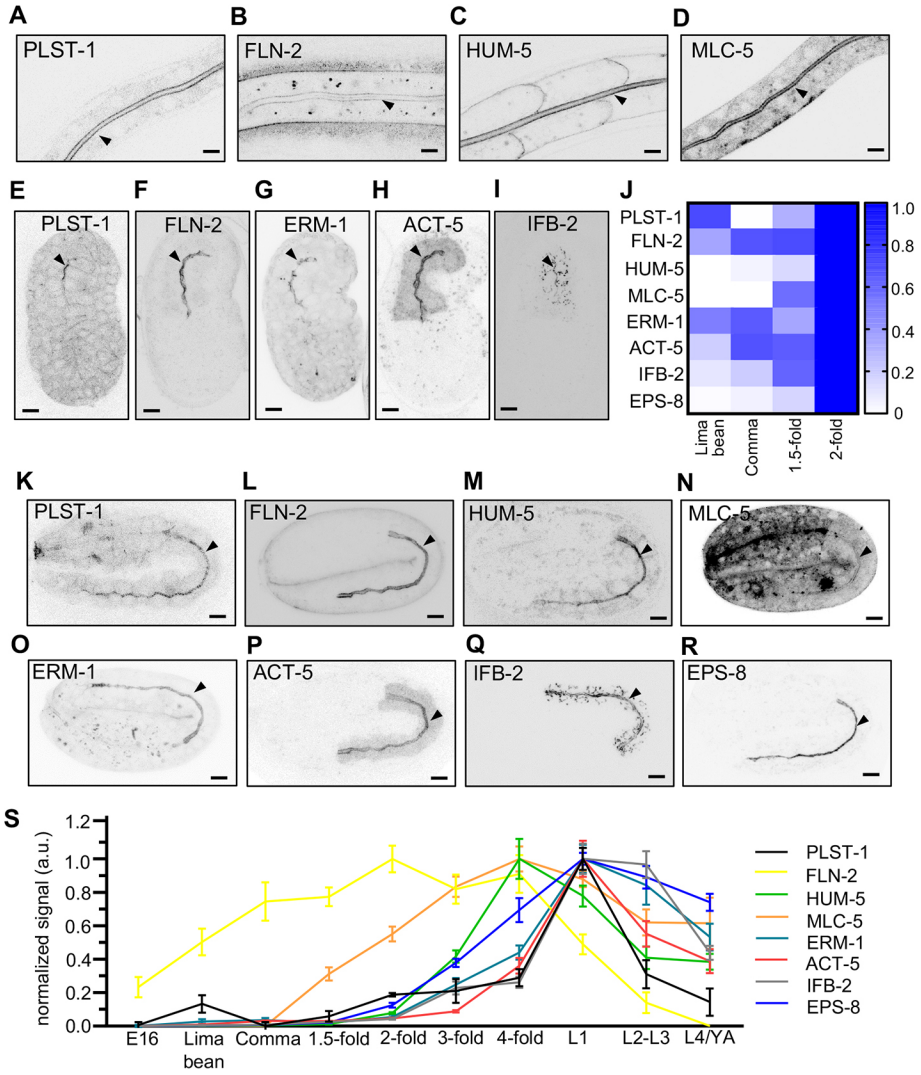


**Fig. 2. Brush border components are dynamically enriched at the apical membrane during microvilli assembly.** (A-I) Representative images of the apical localization of GFP-tagged MLC-5, PLST-1 and ACT-5, mNG-tagged ERM-1, IFB-2 and HUM-5, and mVenus-tagged FLN-2 in L1/L2 larvae (A-D) and lima bean embryos (E-I). (J) The absolute apical signal of the indicated markers was measured on at least ten embryos at each developmental stage. The heatmap shows a focus on early brush border assembly steps where the maximum intensity was set at the 2-fold-stage. (K-R) Apical localization of the indicated markers at the 2-fold stage. (S) The absolute apical localization of the indicated markers was recorded as in J and normalized to the maximum expression for each marker. Data are mean ±s.e.m. a.u., arbitrary units. In all images, arrowheads show the apical plasma membrane of the intestinal cells. Scale bars: 5 µm.

Notably, we found that PLST-1 localized at the bottom of the microvilli (Fig. 3F), with a dotted pattern that was different from the linear endotube pattern (IFB-2 in Fig. 3E). This localization is consistent with that of plastin 1 in mouse and its proposed role in anchoring actin rootlets (Grimm-Gunter et al., 2009). Whereas FLN-2 was hardly detectable in adult worms, we observed in L1 larvae that FLN-2 localized at the base of microvilli, similar to MLC-5, which also partly decorated the whole microvilli (Fig. 3G,H). Finally, we found that HUM-5 localized at both the base and the tip of microvilli, as well as marginally along their length (Fig. 3I), as observed in mouse intestine for Myo1d (Benesh et al., 2010).

Because factors needed to build the microvilli are concomitantly recruited to the apical pole (Fig. 2), we investigated whether super-resolution imaging could resolve the change in their relative microvillar position during brush border assembly. Line scans showed that ERM-1, EPS-8 and IFB-2 colocalized at the beginning of microvilli assembly (2-fold stage) and progressively moved away to end up with IFB-2 and EPS-8 contralaterally positioned and surrounding ERM-1 (Fig. 3J,K, Fig. S4D).

### Analysis of brush border markers dynamics during microvilli assembly

We next analyzed the dynamics of microvillar components during and after brush border establishment using FRAP. Whereas ERM-1 was very dynamic in 1.5-fold embryos, which likely reflects its involvement in microvilli pre-assembly, it became surprisingly stable in the established brush border (adult worm), with little recovery even after >15 min (Fig. 4A, Fig. S5A), confirming recent observations (Ramalho et al., 2020; Remmelzwaal et al., 2021). Analysis of ERM-1 fluorescence recovery throughout *C. elegans* development confirmed that ERM-1 dynamics progressively decreased concomitantly with brush border assembly and became almost static in larvae and adults (Fig. 4B,F,G). To confirm this, the dynamics of other structural components of the brush border was analyzed during microvilli pre-assembly (comma/1.5-fold), maturation (L1 larvae) and in adult worms; note that owing to embryo movements from the 2-fold stage, late embryonic developmental stages could not be investigated. Like ERM-1, EPS-8 was also very dynamic during microvilli pre-assembly but became highly stable in maturing and mature microvilli (Fig. 4C,F,G). ACT-5 also displayed dynamic behavior, albeit to a lesser extent, that persisted until L1 larvae (Fig. 4D,F,G), in agreement with F-actin mobile fractions in Caco-2 cells (~60%) (Waharte et al., 2005), to finally become stable at adulthood. Conversely, the behavior of intermediate filament IFB-2 was more stable at every developmental stage (Fig. 4E-G), which reflects its anchoring role for growing microvilli (Grimm-Gunter et al., 2009; Geisler et al., 2019). These results indicate that mature microvilli are stable *in vivo*. The

Development (2021) 148, dev200029. doi:10.1242/dev.200029

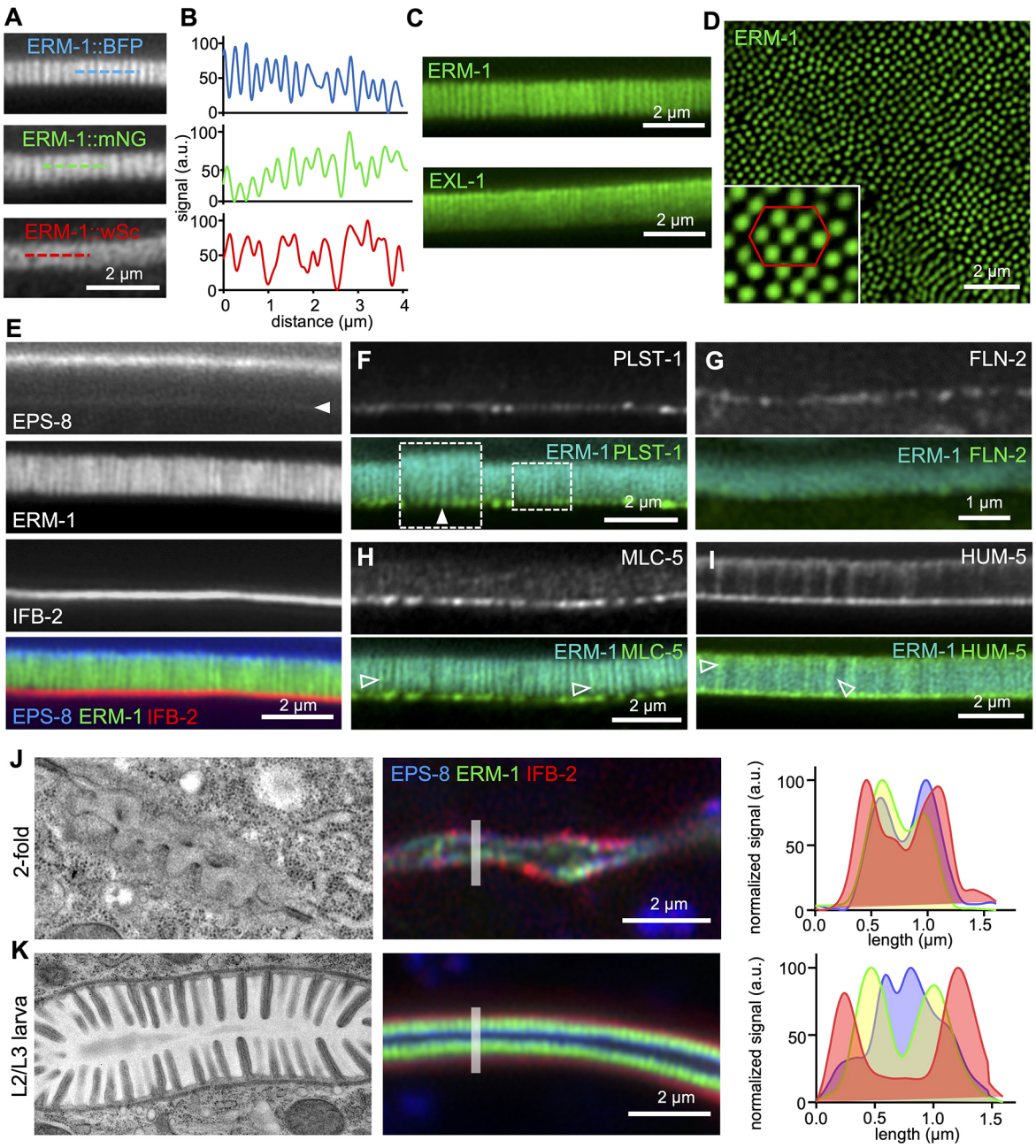


**Fig. 3. Super-resolution imaging of the brush border.** (A,B) Super-resolution images of ERM-1 endogenously tagged with BFP, mNG and wSc in *C. elegans* young adults. The graphs in B show the normalized intensity profile along a 4 µm-long dashed line, as represented in A. (C) Super-resolution images of ERM-1::mNG or EXL-1::mNG in young adults. (D) Transversal super-resolution image of the brush border performed on a young adult *C. elegans* strain endogenously expressing ERM-1::mNG. Inset shows a magnified region with a red hexagon indicating the putative hexagonal packing of microvilli. (E-I) Representative super-resolution images of the indicated microvilli markers endogenously tagged with mNG (ERM-1, HUM-5), GFP (PLST-1, MLC-5), BFP (EPS-8), mVenus (FLN-2) or wSc (IFB-2) in young adults. In F, inset shows higher magnification of the boxed ROI. Filled and unfilled arrowheads show the colocalization between ERM-1 and the indicated markers at the base and along the microvilli, respectively. (J,K) Left: TEM images show the shape of the brush border at the corresponding developmental stage. Middle: Super-resolution images of the brush border in 2-fold embryo and L2-L3 larvae co-expressing EPS-8::BFP, ERM-1::mNG and IFB-2::wSc. Right: Histograms corresponding to the signal intensity profile of the three markers along the gray line depicted on the fluorescence images. a.u., arbitrary units.

maturation status of the brush border might be a key consideration in reconciling conflicting data of the literature. Indeed, immature microvilli in non-polarized cells seem to be more dynamic, i.e. life-cycle of ∼12 min in A6 cells (Gorelik et al., 2003), with intense actin treadmilling (half-time recovery of ezrin of ∼30 s) (Garbett and Bretscher, 2012); in contrast, microvilli have been found to last up to 12 h in mature brush borders (Meenderink et al., 2019). This high stability could partially explain their uniform length and highly ordered organization in the human intestine (Crawley et al., 2014a).

In conclusion, this study shows for the first time the dynamic recruitment of microvilli components during brush border development and their localization at the individual microvillus level *in vivo*. This new toolbox will be instrumental in addressing the many remaining questions regarding microvilli assembly and maturation, notably determining the full set of factors required for

Development (2021) 148, dev200029. doi:10.1242/dev.200029

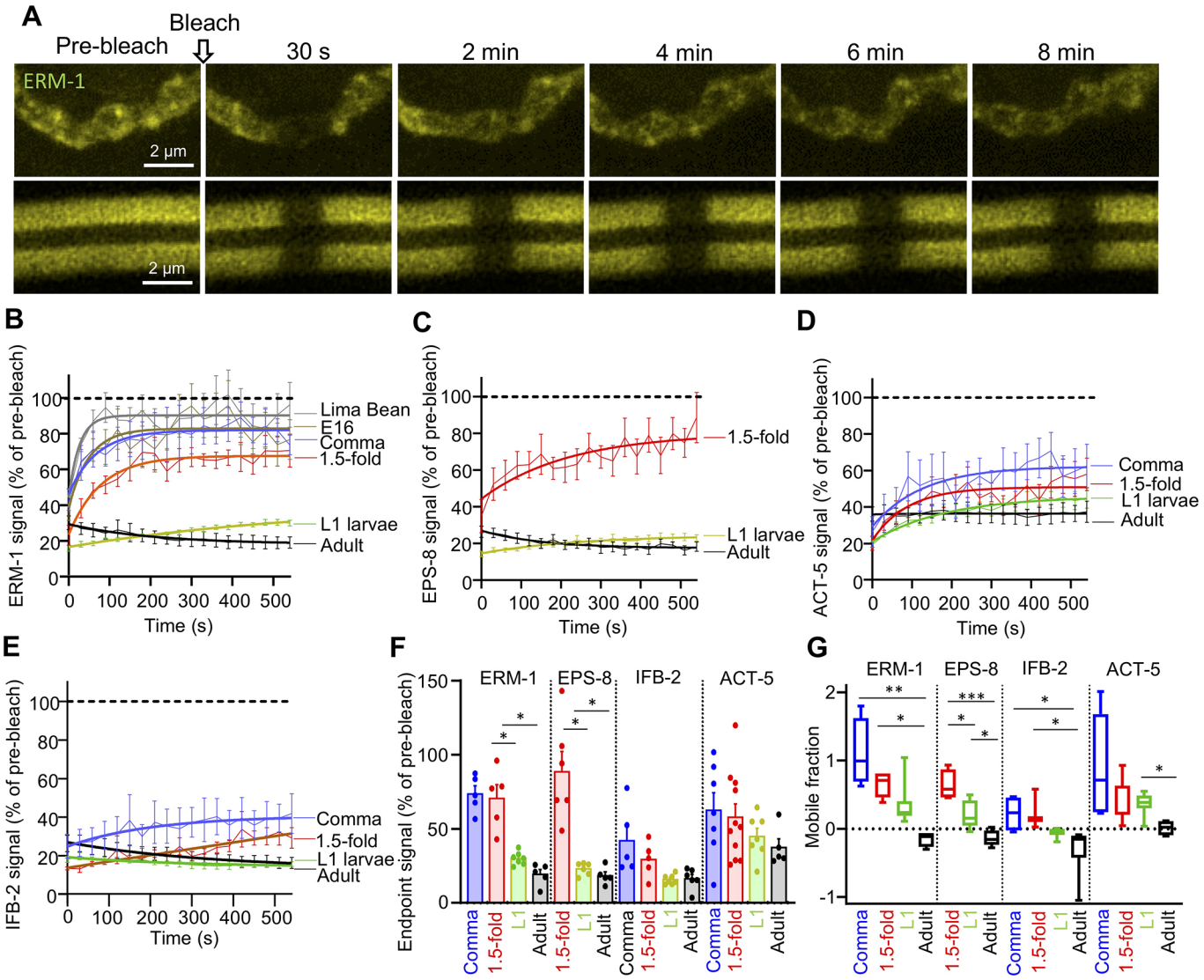


**Fig. 4. Brush border components dynamics during microvilli assembly.** (A) ERM-1::mNG was bleached in a 1.5-fold embryo and an adult worm, and fluorescence recovery was observed every 30 s. (B-E) Quantification of the signal recovery after bleaching of ERM-1::mNG (B), EPS-8::mNG (C), ACT-5::GFP (D) and IFB-2::mNG (E), measured every 30 s on 5-11 worms at the indicated developmental stages. Thin lines represent the mean±s.e.m. of signal recovery, bold lines represent one-phase association non-linear regression fitting curves. (F,G) Analysis of the FRAP experiments shown in B-E at the comma, 1.5-fold, L1 larva and adult stages. F shows the percentage of the pre-bleached signal (mean of two time points) recovered at the endpoint (540 s) and G shows the mobile fraction. Histograms show the mean±s.e.m., dots in F represent individual worms. The difference between variance was calculated using ANOVA, **P*<0.05, ***P*<0.01, ****P*<0.001.

microvilli growth and maintenance, and the principles that govern microvilli size, packing and organization *in vivo*. It will also be essential to understand the pathophysiology of aging and of genetic, inflammatory or pathogenic diseases affecting the brush border.

## MATERIALS AND METHODS

### *C. elegans* strains and maintenance

Strains were maintained under typical conditions as described (Brenner, 1974). CRISPR-CAS9-genome edited mTagBFP2, mNeonGreen and mScarlet-tagged proteins were generated at the Biologie de *Caenorhabditis elegans* facility (Universite Lyon 1, UMS3421, Lyon, France). The strains used in this study are listed in Table S1. The sequence of alleles are available from the Dryad Digital Repository (Gregoire, 2021): dryad.qrfj6q5hh.

### *In vivo* confocal imaging in *C. elegans*

For *in vivo* imaging, *C. elegans* larvae were mounted on a 10% agarose pad in a solution of 100 nm polystyrene microbeads (Polysciences) to stop worm movement. Embryos were mounted on a 2% agarose pad with a mix of bacteria and M9 medium (localization) or M9 only (live imaging). Single confocal slices of the anterior intestinal cells or stacks of the whole intestine were performed on adults/larvae and whole embryos, respectively, using a Leica SP8 (Wetzlar) equipped with a 63×, 1.4 NA objective (LAS AF software) or a super-resolution Zeiss LSM880-Airyscan (Oberkochen) equipped with a 63×, 1.4 NA objective (Zen Black software). For the image in Fig. 3D, young adult animals were quashed to let the intestine out and have a large imaging surface. Quantitative recording of the apical localization of brush border markers was performed on the Leica SP8 microscope using the photon-counting function of HyD hybrid detectors and image accumulation (Fig. S3). For embryos, stacks were reconstructed using the max intensity *z*-projection function of Fiji software (https://imagej.net/Fiji). All images were examined using Fiji software.

### TEM

Samples were subjected to high-pressure freezing followed by freeze substitution, flat embedding, targeting and sectioning using the positional

Development (2021) 148, dev200029. doi:10.1242/dev.200029

correlation and tight trimming approach, as described previously (Bidaud-Meynard et al., 2019). Each embryo or larva was sectioned in five to ten different places, every 5-7 µm, to ensure that different intestinal cells were observed. Ultrathin sections (60-70 nm) were collected on Formvar-coated slot grids (FCF2010-CU, EMS) and observed using a JEM-1400 transmission electron microscope (JEOL) operated at 120 kV, equipped with a Gatan Orius SC 1000 camera (Gatan) and piloted by the Digital Micrograph program.

### FRAP

FRAP experiments were performed using the Zeiss LSM880-Airyscan on a rectangular region of interest (ROI) of 1.3 µm width crossing the apical plasma membrane with 100% 488 nm laser power, 10-20 iterations, and recovery was measured every 30 s for 10-15 min. Post-FRAP images were analyzed using the Fiji software. The mean fluorescence intensity of the bleached ROI was normalized for photobleaching by recording the intensity of the same ROI on a non-bleached region and cytoplasmic background was subtracted on each frame. Finally, the percentage recovery was calculated on each timeframe by comparing the normalized signal intensities with the mean of two time points before bleach. Curve fitting was performed with one-phase association non-linear regression analysis using GraphPad Prism 9 software. The mobile fraction ($Mf$) was calculated with the following equation: $Mf = \frac{I_\infty - I_0}{I_i - I_0}$,
where $I_\infty$ is the signal intensity at the endpoint plateau phase, $I_i$ is the mean of two pre-bleached signal intensities and $I_0$ is the signal intensity at the first post-bleach time point.

### Quantification

TEM micrographs were analyzed using Fiji software and were representative of all the sections observed. Three to five independent worms at each developmental stage were examined in five to ten different sections along the antero-posterior axis. Lumen perimeter was measured around the apical membrane. In total, 32 (2-fold), 36 (3-fold), 31 (4-fold), 26 (L1), 22 (L2/3) and 20 (L4/young adults) lumen perimeters were measured. Microvilli length was measured from the tip to the point where their base intersected with the apical pole. Microvilli width was measured at mid-height. In total, 61 (2-fold), 83 (3-fold), 89 (4-fold), 60 (L1), 62 (L2/3) and 92 (L4/young adults) length and width measurements were performed. Microvilli density was defined as the number of microvilli per unit length of lumen perimeter. In total, 29 (2-fold), 32 (3-fold), 40 (4-fold), 30 (L1), 30 (L2/3) and 40 (L4/young adults) microvilli densities were determined.

For the quantitative measurement of the apical localization of brush border markers, a maximum intensity projection was performed using Fiji, and the signal density was quantified by measuring the mean fluorescence signal along a segmented line covering the whole intestine (E16 to 2-fold embryos) or visible part of the anterior intestine (3-fold to adults). The signal measured was then corrected for fluorescence accumulation and normalized.

### Statistical analysis

Results are presented as mean±s.e.m. of the number of independent experiments indicated in the legends, and scattered dots represent individual worms. $P$-values were calculated by two-tailed, unpaired Student's $t$-test or one-way ANOVA, as indicated in the figure captions, and a 95% confidence level was considered significant. Normal distribution of data and homogeneity of variances were validated using the Shapiro–Wilk and the Bartlett (for ANOVA) or F (for Student's) tests, respectively. Mann–Whitney or Kruskal–Wallis tests were used for calculating the $P$-values between two or multiple non-normal distributions, respectively, and Dunnett's tests was used for multiple distributions with non-homogenous variances.

#### Acknowledgements

We thank Marc Tramier and Stéphanie Dutertre for their advice on fluorescence quantification and super-resolution imaging, respectively, as well as Matis Soleilhac for the initial analysis of expression patterns. We also thank Verena Göbel, Michel Labouesse, Junho Lee and Ronen Zaidel-Bar for strains, Maïté Carre-Pierrat (Biology of *Caenorhabditis elegans* Facility, Universite Lyon 1, UMS3421) for generating CRISPR strains, as well as Céline Burcklé and Guillaume Halet for helpful discussions. Some strains were provided by the CGC, which is funded by NIH Office of Research Infrastructure Programs (P40 OD010440; University of Minnesota, USA). Imaging was performed at the Microscopy Rennes imaging Center (MRiC, Biosit, Rennes, France), a member of the national infrastructure France-BioImaging supported by the French National Research Agency (ANR-10-INBS-04).

#### Competing interests

The authors declare no competing or financial interests.

#### Author contributions

Conceptualization: A.B.-M., G.M.; Methodology: A.B.-M., F.D., O.N., A.P., G.M.; Validation: A.B.-M., F.D., O.N., A.P., G.M.; Formal analysis: A.B.-M., F.D., O.N., A.P., G.M.; Investigation: A.B.-M., F.D., O.N., A.P., G.M.; Resources: S.K.S., C.N.P., F.B.R.; Data curation: A.B.-M., F.D., O.N., A.P., G.M.; Writing - original draft: A.B.-M., G.M.; Writing - review & editing: A.B.-M., O.N., A.P., G.M.; Visualization: A.B.-M., G.M.; Supervision: G.M.; Project administration: G.M.; Funding acquisition: A.B.-M., G.M.

#### Funding

This work was supported by the European Union's Horizon 2020 research and innovation program under a Marie Sklodowska-Curie Actions grant agreement (844070 to A.B.-M.), Défis scientifiques de l'Université de Rennes 1 (17CQ436-S0 to A.B.-M. and G.M.), Ligue Contre le Cancer 22, 29, 35, 41, 72, 85 and the Fondation Maladies Rares (169608 and EXM-2019-1013 to G.M.). The G.M. laboratory also received institutional funding from the Centre National De La Recherche Scientifique and the Université de Rennes 1.

#### Data availability

The sequences of alleles available from the Dryad Digital Repository (Gregoire, 2021): dryad.qrfj6q5hh.

#### Peer review history

The peer review history is available online at https://journals.biologists.com/dev/article-lookup/doi/10.1242/dev.200029.

#### References

**Achilleos, A., Wehman, A. M. and Nance, J.** (2010). PAR-3 mediates the initial clustering and apical localization of junction and polarity proteins during C. elegans intestinal epithelial cell polarization. *Development* **137**, 1833-1842. doi:10.1242/dev.047647

**Altun, Z. F. and Hall, D. H.** (2009). Handbook of C. elegans Anatomy. In *WormAtlas*. http://www.wormatlas.org/hermaphrodite/hermaphroditehomepage.htm

**Asan, A., Raiders, S. A. and Priess, J. R.** (2016). Morphogenesis of the C. elegans intestine involves axon guidance genes. *PLoS Genet.* **12**, e1005950. doi:10.1371/journal.pgen.1005950

**Benesh, A. E., Nambiar, R., Mcconnell, R. E., Mao, S., Tabb, D. L. and Tyska, M. J.** (2010). Differential localization and dynamics of class I myosins in the enterocyte microvillus. *Mol. Biol. Cell* **21**, 970-978. doi:10.1091/mbc.e09-07-0638

**Bidaud-Meynard, A., Nicolle, O., Heck, M., Le Cunff, Y. and Michaux, G.** (2019). A V0-ATPase-dependent apical trafficking pathway maintains the polarity of the intestinal absorptive membrane. *Development* **146**, dev174508. doi:10.1242/dev.174508

**Bossinger, O., Fukushige, T., Claeys, M., Borgonie, G. and Mcghee, J. D.** (2004). The apical disposition of the Caenorhabditis elegans intestinal terminal web is maintained by LET-413. *Dev. Biol.* **268**, 448-456. doi:10.1016/j.ydbio.2004.01.003

**Brenner, S.** (1974). The genetics of Caenorhabditis elegans. *Genetics* **77**, 71-94. doi:10.1093/genetics/77.1.71

**Chang, J., Chance, M. R., Nicholas, C., Ahmed, N., Guilmeau, S., Flandez, M., Wang, D., Byun, D. S., Nasser, S., Albanese, J. M. et al.** (2008). Proteomic changes during intestinal cell maturation in vivo. *J. Proteomics* **71**, 530-546. doi:10.1016/j.jprot.2008.08.003

**Chinowsky, C. R., Pinette, J. A., Meenderink, L. M., Lau, K. S. and Tyska, M. J.** (2020). Nonmuscle myosin-2 contractility-dependent actin turnover limits the length of epithelial microvilli. *Mol. Biol. Cell* **31**, 2803-2815. doi:10.1091/mbc.E20-09-0582

**Cordova-Burgos, L., Patel, F. B. and Soto, M. C.** (2021). E-Cadherin/HMR-1 membrane enrichment is polarized by WAVE-dependent branched actin. *J Dev Biol* **9**, 19. doi:10.3390/jdb9020019

**Crawley, S. W., Mooseker, M. S. and Tyska, M. J.** (2014a). Shaping the intestinal brush border. *J. Cell Biol.* **207**, 441-451. doi:10.1083/jcb.201407015

**Crawley, S. W., Shifrin, D. A., Jr, Grega-Larson, N. E., Mcconnell, R. E., Benesh, A. E., Mao, S., Zheng, Y., Zheng, Q. Y., Nam, K. T., Millis, B. A. et al.**

(2014b). Intestinal brush border assembly driven by protocadherin-based intermicrovillar adhesion. *Cell* **157**, 433-446. doi:10.1016/j.cell.2014.01.067

**Croce, A., Cassata, G., Disanza, A., Gagliani, M. C., Tacchetti, C., Malabarba, M. G., Carlier, M. F., Scita, G., Baumeister, R. and Di Fiore, P. P.** (2004). A novel actin barbed-end-capping activity in EPS-8 regulates apical morphogenesis in intestinal cells of Caenorhabditis elegans. *Nat. Cell Biol.* **6**, 1173-1179. doi:10.1038/ncb1198

**El Mouridi, S., Lecroisey, C., Tardy, P., Mercier, M., Leclercq-Blondel, A., Zariohi, N. and Boulin, T.** (2017). Reliable CRISPR/Cas9 genome engineering in caenorhabditis elegans using a single efficient sgRNA and an easily recognizable phenotype. *G3 (Bethesda)* **7**, 1429-1437. doi:10.1534/g3.117.040824

**Faust, J. J., Millis, B. A. and Tyska, M. J.** (2019). Profilin-mediated actin allocation regulates the growth of epithelial microvilli. *Curr. Biol.* **29**, 3457-3465.e3. doi:10.1016/j.cub.2019.08.051

**Feldman, J. L. and Priess, J. R.** (2012). A role for the centrosome and PAR-3 in the hand-off of MTOC function during epithelial polarization. *Curr. Biol.* **22**, 575-582. doi:10.1016/j.cub.2012.02.044

**Fili, N. and Toseland, C. P.** (2019). Unconventional myosins: how regulation meets function. *Int. J. Mol. Sci.* **21**, 67. doi:10.3390/ijms21010067

**Gaeta, I. M., Meenderink, L. M., Postema, M. M., Cencer, C. S. and Tyska, M. J.** (2021). Direct visualization of epithelial microvilli biogenesis. *Curr. Biol.* **31**, 2561-2575.e6. doi:10.1016/j.cub.2021.04.012

**Gally, C., Wissler, F., Zahreddine, H., Quintin, S., Landmann, F. and Labouesse, M.** (2009). Myosin II regulation during C. elegans embryonic elongation: LET-502/ROCK, MRCK-1 and PAK-1, three kinases with different roles. *Development* **136**, 3109-3119. doi:10.1242/dev.039412

**Garbett, D. and Bretscher, A.** (2012). PDZ interactions regulate rapid turnover of the scaffolding protein EBP50 in microvilli. *J. Cell Biol.* **198**, 195-203. doi:10.1083/jcb.201204008

**Geisler, F., Coch, R. A., Richardson, C., Goldberg, M., Denecke, B., Bossinger, O. and Leube, R. E.** (2019). The intestinal intermediate filament network responds to and protects against microbial insults and toxins. *Development* **146**, dev169482. doi:10.1242/dev.169482

**Geisler, F., Coch, R. A., Richardson, C., Goldberg, M., Bevilacqua, C., Prevedel, R. and Leube, R. E.** (2020). Intestinal intermediate filament polypeptides in C. elegans: Common and isotype-specific contributions to intestinal ultrastructure and function. *Sci. Rep.* **10**, 3142. doi:10.1038/s41598-020-59791-w

**Gobel, V., Barrett, P. L., Hall, D. H. and Fleming, J. T.** (2004). Lumen morphogenesis in C. elegans requires the membrane-cytoskeleton linker erm-1. *Dev Cell* **6**, 865-873. doi:10.1016/j.devcel.2004.05.018

**Gorelik, J., Shevchuk, A. I., Frolenkov, G. I., Diakonov, I. A., Lab, M. J., Kros, C. J., Richardson, G. P., Vodyanoy, I., Edwards, C. R., Klenerman, D. et al.** (2003). Dynamic assembly of surface structures in living cells. *Proc. Natl. Acad. Sci. U.S.A.* **100**, 5819-5822. doi:10.1073/pnas.1030502100

**Gregoire, M.** (2021). High resolution dynamic mapping of the C. elegans intestinal brush border. *Dryad Dataset*. doi:10.5061/dryad.qrfj6q5hh

**Grimm-Gunter, E. M., Revenu, C., Ramos, S., Hurbain, I., Smyth, N., Ferrary, E., Louvard, D., Robine, S. and Rivero, F.** (2009). Plastin 1 binds to keratin and is required for terminal web assembly in the intestinal epithelium. *Mol. Biol. Cell* **20**, 2549-2562. doi:10.1091/mbc.e08-10-1030

**Houdusse, A. and Titus, M. A.** (2021). The many roles of myosins in filopodia, microvilli and stereocilia. *Curr. Biol.* **31**, R586-R602. doi:10.1016/j.cub.2021.04.005

**Hunt-Newbury, R., Viveiros, R., Johnsen, R., Mah, A., Anastas, D., Fang, L., Halfnight, E., Lee, D., Lin, J., Lorch, A. et al.** (2007). High-throughput in vivo analysis of gene expression in Caenorhabditis elegans. *PLoS Biol.* **5**, e237. doi:10.1371/journal.pbio.0050237

**Leung, B., Hermann, G. J. and Priess, J. R.** (1999). Organogenesis of the Caenorhabditis elegans intestine. *Dev. Biol.* **216**, 114-134. doi:10.1006/dbio.1999.9471

**Liang, J., Shaulov, Y., Savage-Dunn, C., Boissinot, S. and Hoque, T.** (2017). Chloride intracellular channel proteins respond to heat stress in Caenorhabditis elegans. *PLoS ONE* **12**, e0184308. doi:10.1371/journal.pone.0184308

**Loveless, T. and Hardin, J.** (2012). Cadherin complexity: recent insights into cadherin superfamily function in C. elegans. *Curr. Opin. Cell Biol.* **24**, 695-701. doi:10.1016/j.ceb.2012.06.008

**MacQueen, A. J., Baggett, J. J., Perumov, N., Bauer, R. A., Januszewski, T., Schriefer, L. and Waddle, J. A.** (2005). ACT-5 is an essential Caenorhabditis elegans actin required for intestinal microvilli formation. *Mol. Biol. Cell* **16**, 3247-3259. doi:10.1091/mbc.e04-12-1061

**Mangeat, T., Labouesse, S., Allain, M., Negash, A., Martin, E., Guénolé, A., Poincloux, R., Estibal, C., Bouissou, A., Cantaloube, S. et al.** (2021). Super-resolved live-cell imaging using random illumination microscopy. *Cell Reports Methods* **1**, 100009. doi:10.1016/j.crmeth.2021.100009

**Mariadason, J. M., Nicholas, C., L'italien, K. E., Zhuang, M., Smartt, H. J., Heerdt, B. G., Yang, W., Corner, G. A., Wilson, A. J., Klampfer, L. et al.** (2005). Gene expression profiling of intestinal epithelial cell maturation along the crypt-villus axis. *Gastroenterology* **128**, 1081-1088. doi:10.1053/j.gastro.2005.01.054

**Mcconnell, R. E., Benesh, A. E., Mao, S., Tabb, D. L. and Tyska, M. J.** (2011). Proteomic analysis of the enterocyte brush border. *Am. J. Physiol. Gastrointest. Liver Physiol.* **300**, G914-G926. doi:10.1152/ajpgi.00005.2011

**Meenderink, L. M., Gaeta, I. M., Postema, M. M., Cencer, C. S., Chinowsky, C. R., Krystofiak, E. S., Millis, B. A. and Tyska, M. J.** (2019). Actin dynamics drive microvillar motility and clustering during brush border assembly. *Dev. Cell* **50**, 545-556.e4. doi:10.1016/j.devcel.2019.07.008

**Nicolle, O., Burel, A., Griffiths, G., Michaux, G. and Kolotuev, I.** (2015). Adaptation of cryo-sectioning for IEM labeling of asymmetric samples: a study using caenorhabditis elegans. *Traffic* **16**, 893-905. doi:10.1111/tra.12289

**Postema, M. M., Grega-Larson, N. E., Neininger, A. C. and Tyska, M. J.** (2018). IRTKS (BAIAP2L1) elongates epithelial microvilli using EPS8-dependent and independent mechanisms. *Curr. Biol.* **28**, 2876-2888.e4. doi:10.1016/j.cub.2018.07.022

**Ramalho, J. J., Sepers, J. J., Nicolle, O., Schmidt, R., Cravo, J., Michaux, G. and Boxem, M.** (2020). C-terminal phosphorylation modulates ERM-1 localization and dynamics to control cortical actin organization and support lumen formation during Caenorhabditis elegans development. *Development* **147**, dev188011. doi:10.1242/dev.188011

**Remmelzwaal, S., Geisler, F., Stucchi, R., Van Der Horst, S., Pasolli, M., Kroll, J. R., Jarosinska, O. D., Akhmanova, A., Richardson, C. A., Altelaar, M. et al.** (2021). BBLN-1 is essential for intermediate filament organization and apical membrane morphology. *Curr. Biol.* **31**, 2334-2346.e9. doi:10.1016/j.cub.2021.03.069

**Sato, K., Norris, A., Sato, M. and Grant, B. D.** (2014). C. elegans as a model for membrane traffic. *WormBook* **25**, 1-47. doi:10.1895/wormbook.1.77.2

**Sauvanet, C., Wayt, J., Pelaseyed, T. and Bretscher, A.** (2015). Structure, regulation, and functional diversity of microvilli on the apical domain of epithelial cells. *Annu. Rev. Cell Dev. Biol.* **31**, 593-621. doi:10.1146/annurev-cellbio-100814-125234

**Shaner, N. C., Lambert, G. G., Chammas, A., Ni, Y., Cranfill, P. J., Baird, M. A., Sell, B. R., Allen, J. R., Day, R. N., Israelsson, M. et al.** (2013). A bright monomeric green fluorescent protein derived from Branchiostoma lanceolatum. *Nat. Methods* **10**, 407-409. doi:10.1038/nmeth.2413

**Subach, O. M., Cranfill, P. J., Davidson, M. W. and Verkhusha, V. V.** (2011). An enhanced monomeric blue fluorescent protein with the high chemical stability of the chromophore. *PLoS One* **6**, e28674. doi:10.1371/journal.pone.0028674

**Van Furden, D., Johnson, K., Segbert, C. and Bossinger, O.** (2004). The C. elegans ezrin-radixin-moesin protein ERM-1 is necessary for apical junction remodelling and tubulogenesis in the intestine. *Dev. Biol.* **272**, 262-276. doi:10.1016/j.ydbio.2004.05.012

**Vogel, G. F., Klee, K. M., Janecke, A. R., Muller, T., Hess, M. W. and Huber, L. A.** (2015). Cargo-selective apical exocytosis in epithelial cells is conducted by Myo5B, Slp4a, Vamp7, and Syntaxin 3. *J. Cell Biol.* **211**, 587-604. doi:10.1083/jcb.201506112

**Waharte, F., Brown, C. M., Coscoy, S., Coudrier, E. and Amblard, F.** (2005). A two-photon FRAP analysis of the cytoskeleton dynamics in the microvilli of intestinal cells. *Biophys. J.* **88**, 1467-1478. doi:10.1529/biophysj.104.049619

**Zhang, R. and Hou, A.** (2013). Host-Microbe Interactions in Caenorhabditis elegans. *ISRN Microbiol.* **2013**, 356451. doi:10.1155/2013/356451

**Zhang, H., Kim, A., Abraham, N., Khan, L. A. and Gobel, V.** (2013). Vesicular sorting controls the polarity of expanding membranes in the C. elegans intestine. *Worm* **2**, e23702. doi:10.4161/worm.23702

**Zhou, X., Massol, R. H., Nakamura, F., Chen, X., Gewurz, B. E., Davis, B. M., Lencer, W. I. and Waldor, M. K.** (2014). Remodeling of the intestinal brush border underlies adhesion and virulence of an enteric pathogen. *mBio* **5**, e01639-14. doi:10.1128/mBio.01639-14

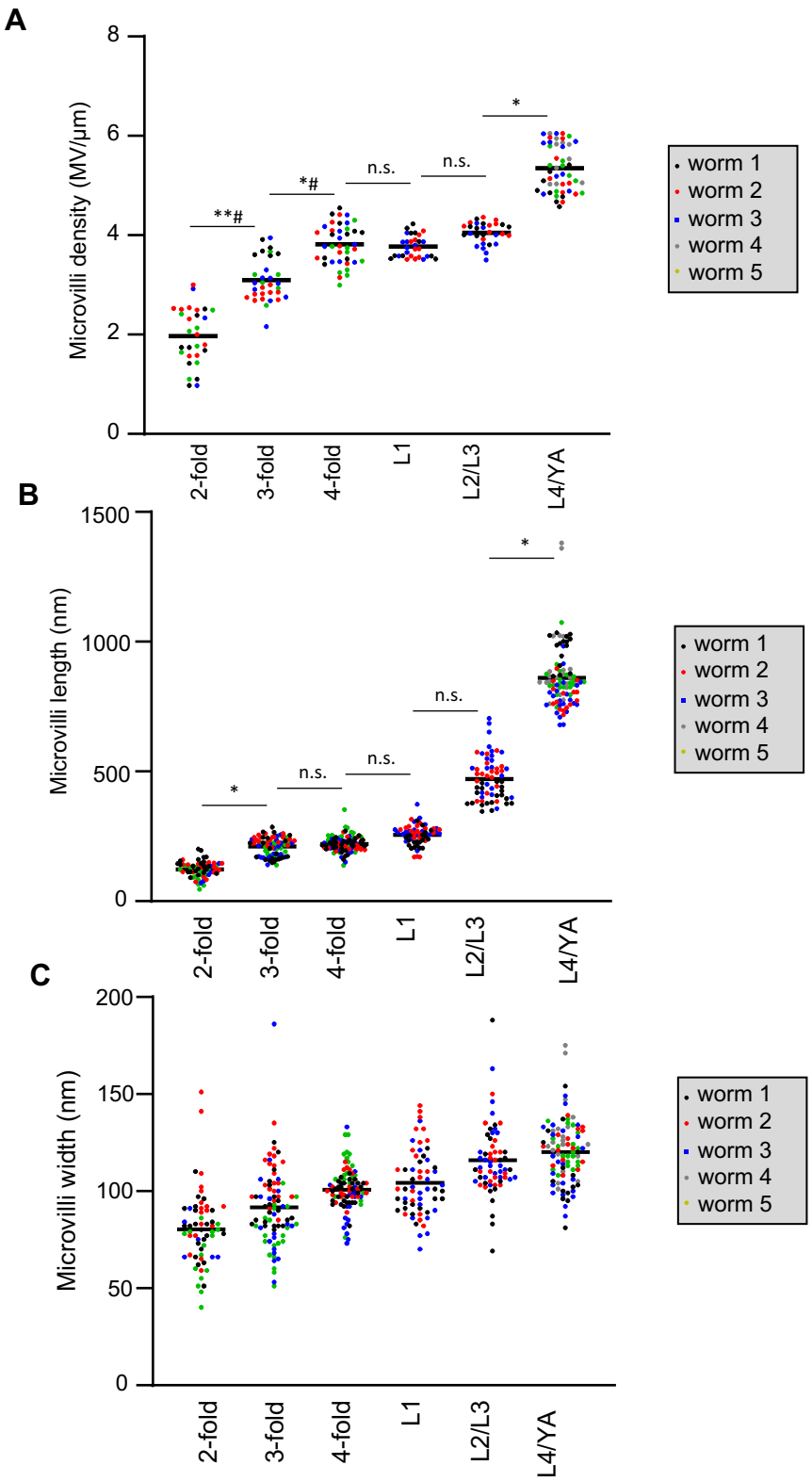


**Fig. S1. Individual values of brush border measurements by TEM, related to Fig. 1.**
Colorized dots represent individual worms at the indicated developmental stages. Bar is the grand mean of all the measurements. Microvilli density was measured on 3-13 slices/worm, microvilli length and width on 6-29 microvilli/worm. N.s., non-significant, *p<0,05, **p<0,01. Except in A, where some data were analysed by unpaired t-test (#), statistical significance was calculated using Mann-Whitney test.

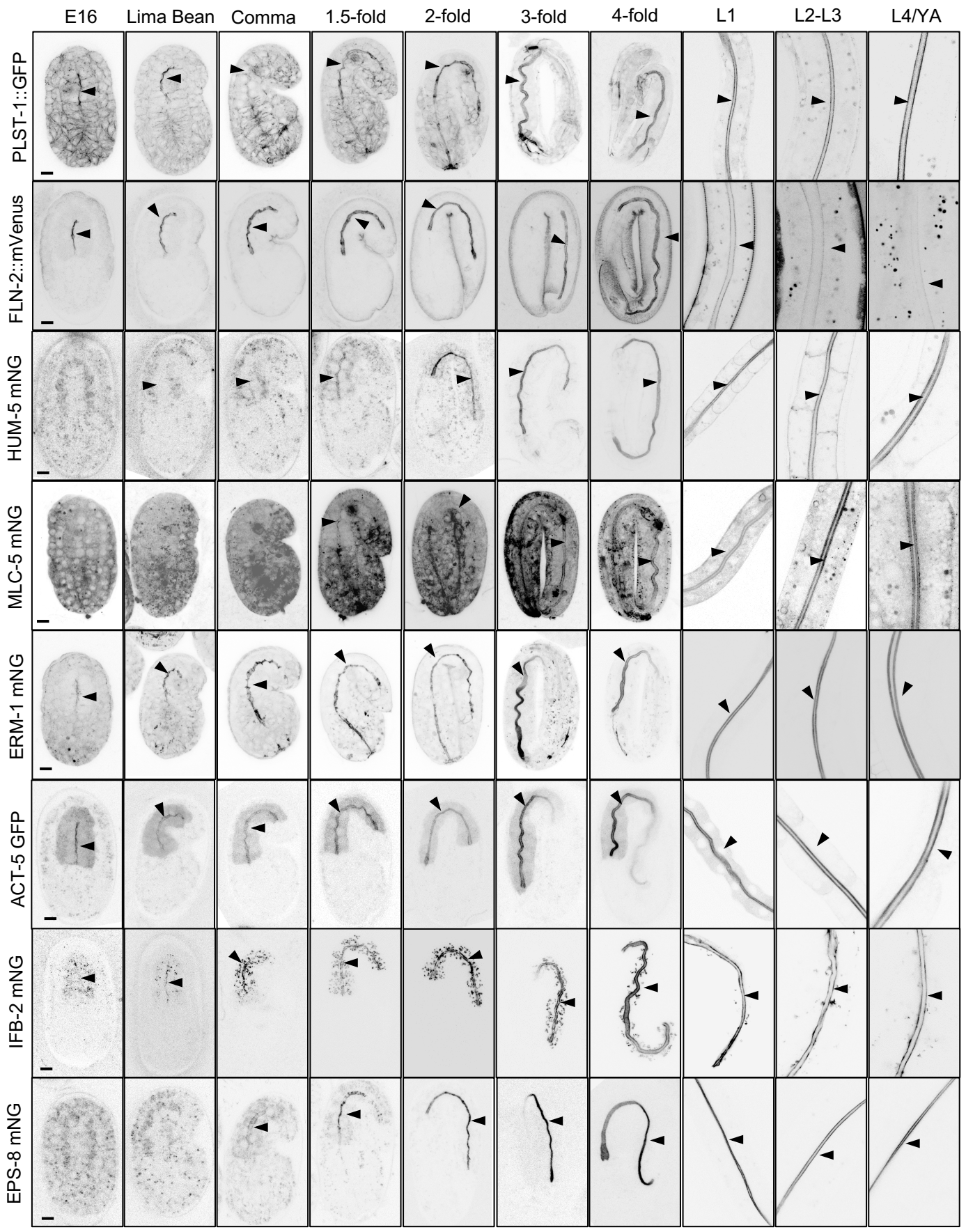


**Fig. S2. Systematic analysis of brush border markers during *C. elegans* development.** Representative confocal images of the endogenously tagged markers indicated (except ACT-5::GFP). Arrowheads show the intestinal cells apical PM. Scale bar is 5 µm.

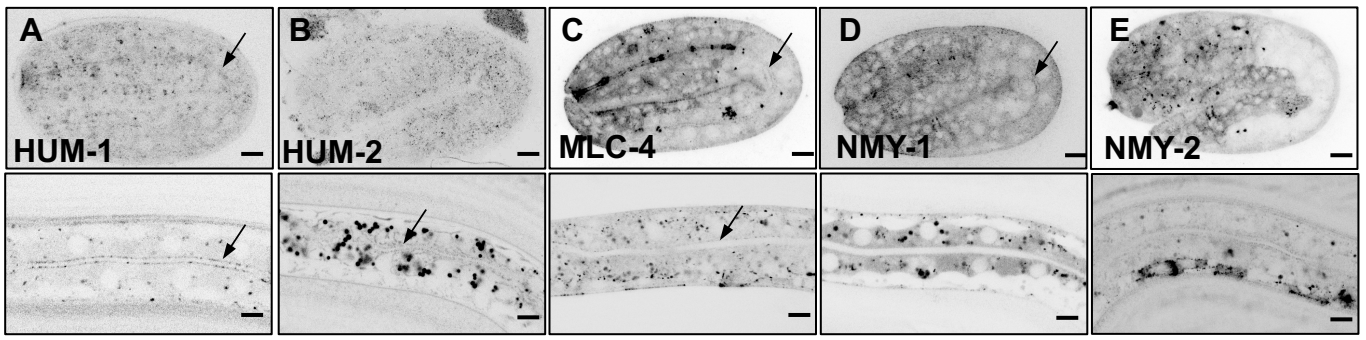


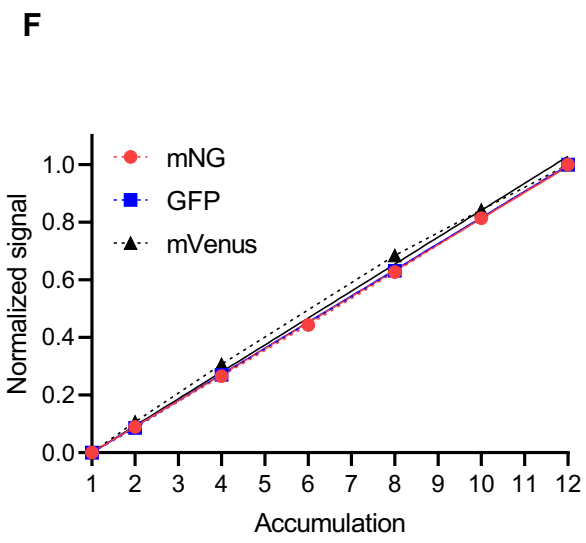


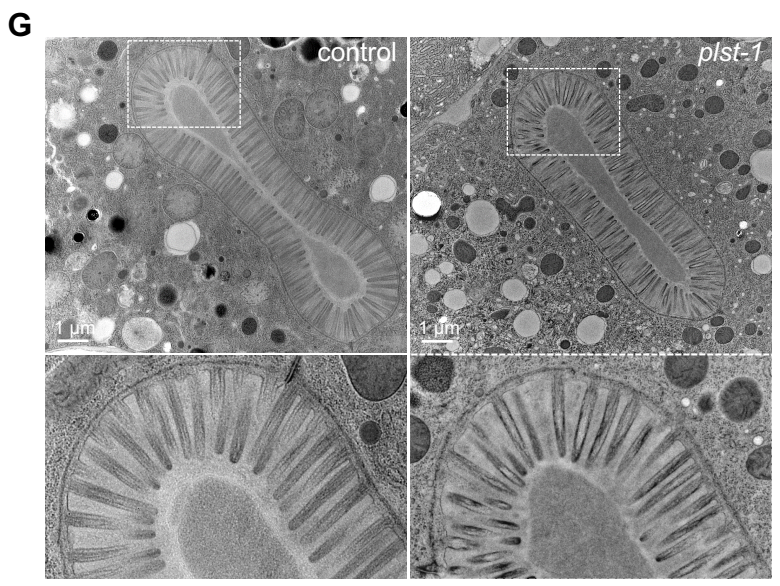


**Fig. S3. Systematic analysis of brush border markers during *C. elegans* development.**
(A-E) Representative confocal images of *C. elegans* strains expressing endogenously tagged versions of the indicated markers, which showed no apical accumulation during *C. elegans* intestine development. Scale bar, 5 µm. (F) Control of the quantitative assessment of brush border markers arrival at the apical PM. Accumulation of IFB-2::mNG, PLST-1::GFP and FLN-2::mVenus signal linearly increases with image accumulation. Experimental points are linked by dashed lines, bold lines show simple linear regression curve fitting. n=1-2 measurement per timepoint for each fluorophore. (G) Representative TEM images of control (N2) and *plst-1(tm4255)* L4/young adult worms (N=3 worms in each condition).

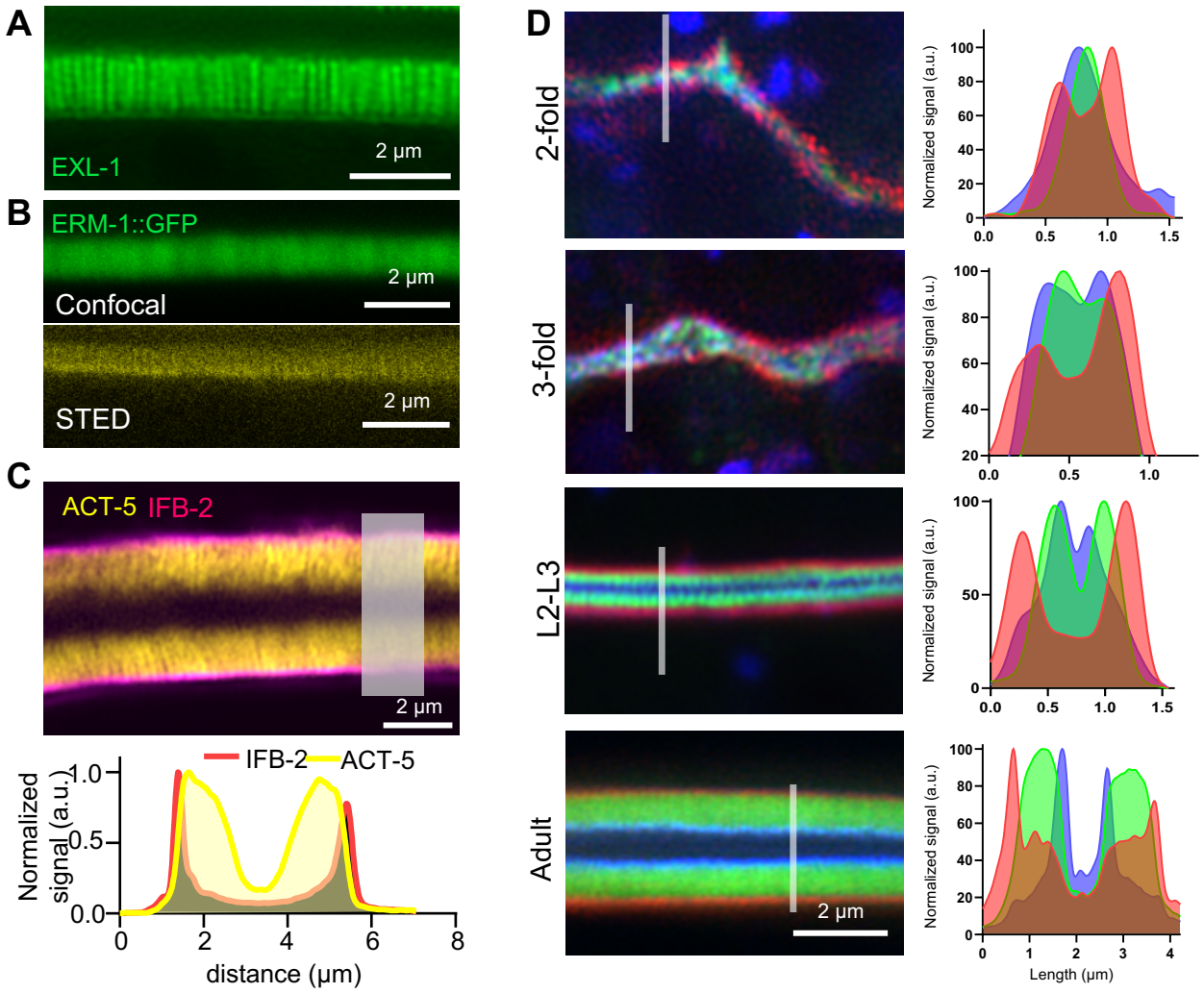


**Fig. S4. Super-resolution imaging of brush border markers *in vivo*.** (A) Representative super-resolution image of exogenously expressed EXL-1::GFP. (B) ERM-1::GFP was imaged in adult worms using the indicated microscopes. (C) Super-resolution images of a *C. elegans* adults co-expressing ACT-5::GFP and IFB-2::wSc. Bottom panel shows a normalized intensity profile along the line depicted in grey. (D) Representative images of the localization of endogenously tagged EPS-8::BFP, ERM-1::mNG and IFB-2::wSc in *C. elegans* at the indicated developmental stages. Right panels show an intensity profile of the three markers along the line depicted in left panels. Scale bars, 2 µm.

.

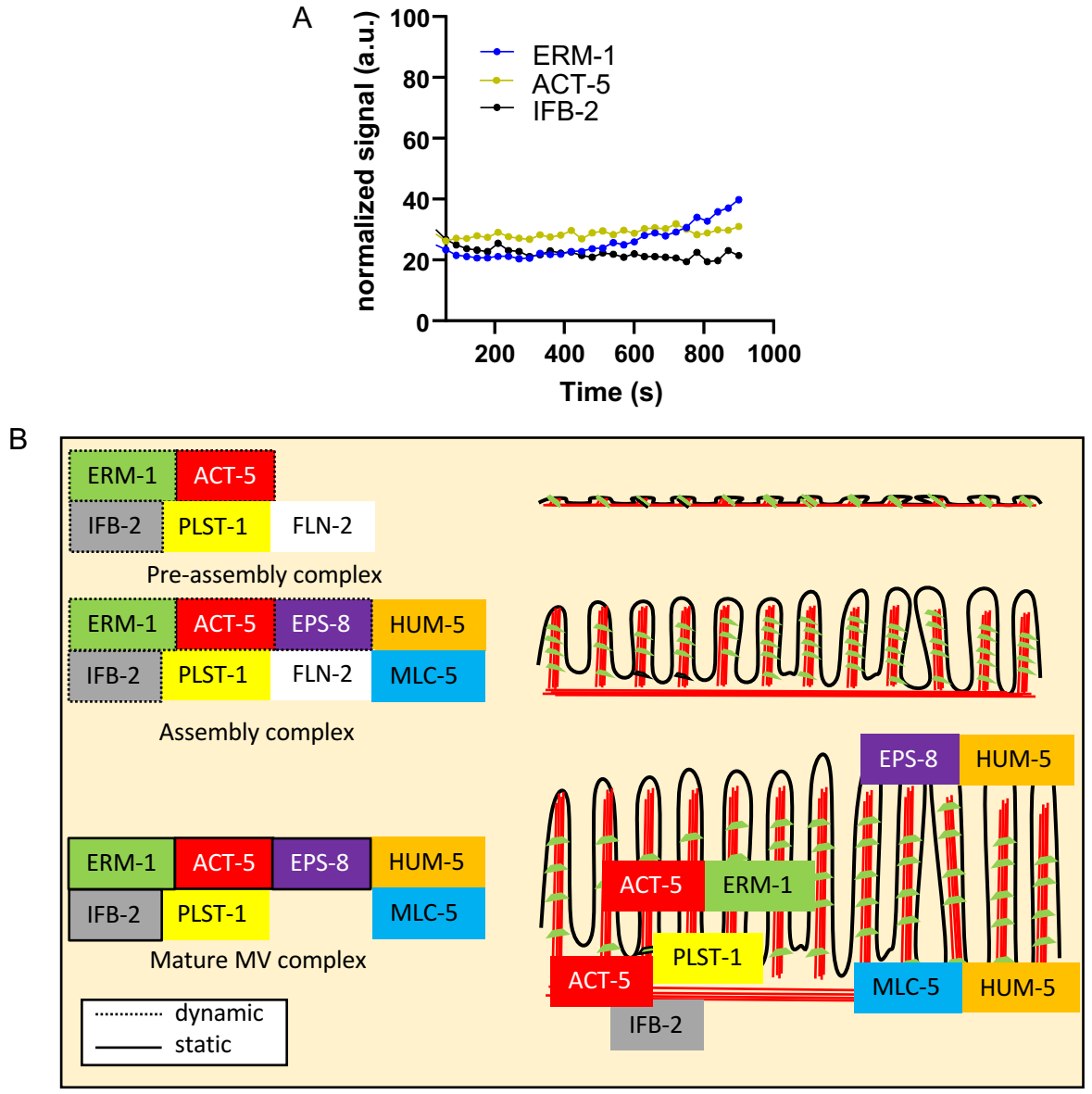


**Fig. S5. Dynamic recruitment of brush border components.**

(A) Longer measurement of brush border components dynamics in adult worms. The curves show the recovery of ERM-1::mNG, IFB-2::mNG and ACT-5::GFP signal every 30 s after photobleaching, measured for an extended time, n=1 for each marker. (B) Model of brush border assembly *in vivo* in *C. elegans*. Microvilli are built from a preformed *pre-assembly complex* and grow through the dynamic recruitment of brush border components, which become highly stable in the mature brush border.

**Table S1. *C. elegans* strains used in this study.**

| Strain | Markers/targets | Genotype | Reference |
|---|---|---|---|
| FBR96 | MLC-4 | mlc-4(jme04[mlc-4::eGFP+loxP]) III | Francois Robin lab |
| FBR140 | MLC-5 | mlc-5(jme09[GFP^3xFLAG::mlc-5]) III | Francois Robin lab |
| FBR222 | FLN-2 | fln-2(jme-19[fln-2::mVenus]) X | Francois Robin lab |
| FL274 | ERM-1, IFB-2 | erm-1(bab59[erm-1::mNG^SEC^3xFlag]) I ; ifb-2(bab142[ifb-2::wSc]) II | Bidaud-Meynard et al., 2019 |
| FL290 | EPS-8 | eps-8(bab140[eps-8::mNG]) IV | This study |
| FL369 | ERM-1, ACT-5 | fgEx13[perm-1::erm-1::gfp + rol-6 (su1006)] ; jyIs17 [vha-6p::mcherry::act-5, ttx-3p::RFP] | Bidaud-Meynard et al., 2019 |
| FL378 | ERM-1 | erm-1(bab59[erm-1::mNG^3xFlag]) I | Bidaud-Meynard et al., 2019 |
| FL379 | ERM-1 | bab64[erm-1::wrmSc^3xFlag] I | Bidaud-Meynard et al., 2019 |
| FL381 | ACT-5, IFB-2 | fgEx12 (act-5p::act-5::gfp); ifb-2(bab142[ifb-2::wrmSc]) II | This study |
| FL383 | EPS-8, ERM-1, IFB-2 | eps-8(bab140[eps-8::mNG]) IV ; erm-1(bab59[erm-1::mNG^SEC^3xFlag]) I; ifb-2(bab142[ifb-2::wSc]) II | This study |
| FL384 | ERM-1 | erm-1(bab167[erm-1::degron-tagBFP2]) I | This study |
| FL385 | IFB-2 | ifb-2(bab153[ifb-2::mNG]) II | This study |
| FL386 | ERM-1, PLST1 | erm-1(bab167[erm-1::degron-tagBFP2]) ; plst-1(msn190[plst-1::gfp]) IV | This study |
| FL387 | ERM1, HUM5 | erm-1(bab167[erm-1::degron-tagBFP2]) ; hum-5(bab189[hum-5::mNG]) III | This study |
| FL388 | ERM-1, MLC5 | erm-1(bab167[erm-1::degron-tagBFP2]) ; mlc-5(jme09[GFP^3xFLAG::mlc-5]) III | This study |
| FL586 | ERM-1, FLN-2 | erm-1(bab167[erm-1::degron-tagBFP2]), fln-2(jme-19[fln-2::mVenus]) X | This study |
| LP162 | NMY-2 | nmy-2(cp13[nmy-2::GFP + LoxP]) I | CGC |
| LP462 | MRCK-1 | mrck-1(cp189[mrck-1::GFP::3xFlag]) V | CGC |
| MCP111 | PGP-1 | pgp-1(bab111[mNG^3xFlag::pgp-1]) IV | Bidaud-Meynard et al., 2019 |
| MCP184 | HUM-2 | hum-2(bab184[hum-2::mNG]) V | This study |
| MCP189 | HUM-5 | hum-5(bab189[hum-5::mNG]) III | This study |
| MCP223 | EXL-1 | exl-1(bab223[exl-1::mNG]) II | This study |
| ML2540 | NMY-1 | nmy-1(mc82[nmy-1::gfp]) X. | Vuong-Brender et al., 2017 |
| OH2211 | EXL-1 | otEx1184 [exl-1p::exl-1::GFP + rol-6(su1006)] | CGC |
| QQ226 | HUM-1 | hum-1(cv21[hum-1::RFP]) I | CGC |
| RZB213 | PLST-1 | plst-1(msn190[plst-1::gfp]) IV | Ding et al., 2017 |
| RZB365 | PLST-1 | plst-1(tm4255) | Ronen Zaidel-Bar lab |
| VJ268 | ACT-5 | fgEx12(act-5p::act-5::gfp) | Zhang et al., 2012 |

**File S1.**

Click here to download Supplementary File 1